Electron Transfer at the Gas−Solid Interface: Reaction of Gas-Phase $MoCl_5$ with Vanadium Oxide Supported on Silica

Karen Malka,[†] Jean Aubard,[‡] Michel Delamar,[‡] Vincent Vivier,[†] Michel Che,[†,§] and Catherine Louis*[,†]

Laboratoire de Réactivité de Surface, UMR CNRS 7609, Université Pierre et Marie Curie, 4 Place Jussieu, 75252 Paris Cedex 05, France, Institut de Topologie et Dynamique des Systèmes (ITODYS), UMR CNRS 7086, Université Paris VII-Denis Diderot, 1 rue Guy de la Brosse, 75251 Paris Cedex 05, France, and Institut Universitaire de France, 103 boulevard Saint-Michel, 75005 Paris, France

Received: October 18, 2002; In Final Form: May 16, 2003

Electron transfer between two transition metals, $MoCl_5$ and VO_x supported on silica, is studied in situ at the gas−solid interface by spectroscopy (electron paramagnetic resonance, diffuse reflectance UV−vis−near-IR, XPS, Raman), electron microscopy, and chemical analysis for a long period of time (∼9000 h). Initially, the VO_x/SiO_2 (V^V, $3d^0$) solid phase is composed of V_2O_5 crystallites and monomeric tetrahedral vanadyl species grafted onto silica ($(\equiv SiO)_3V{=}O$). Upon reaction at 30 °C with gas-phase $MoCl_5$ (Mo^V, $4d^1$), the solid undergoes drastic changes in color, which define four stages. Each stage is accompanied by variations in the chemical state of the supported phase. The principal results are as follows. (i) No electron transfer and no reaction takes place between $MoCl_5$ and grafted $(\equiv SiO)_3V{=}O$ species. (ii) In contrast, V_2O_5 crystallites undergo both electron transfer from Mo^V to V^V and chemical changes leading to a change in the speciation of V and to the formation of a new and amorphous $V^{IV}-O-Mo^{VI}-Cl$ phase. (iii) The following sequence of redox potentials can be proposed for the $MoCl_5-VO_x/SiO_2$ system: $E(V^V/V^{IV})_{V_2O_5\ cryst} > E(Mo^{VI}/Mo^V)_{MoCl_5} > E(V^V/V^{IV})_{(\equiv SiO)_3V=O}$. The difference in behavior of the two types of vanadium species toward electron transfer from $MoCl_5$ is discussed in terms of the dependence of the nature of the ligands, the symmetry, and the nuclearity of the vanadium species on the redox potentials.

Introduction

Electron transfer and redox reactions are well-known in the liquid phase. For instance, in the case of compounds containing vanadium and molybdenum, the reduction by one electron of heteropolyanions of Keggin structure, α-$[SiVMo_{11}O_{40}]^{6-}$ and α-$[PVMo_{11}O_{40}]^{5-}$, leads to the reduction of V^V rather than of Mo^{VI} as attested by electron paramagnetic resonance (EPR).[1] An intervalence charge-transfer band is also observed by UV−vis.[1] These results are consistent with the values of the standard redox potentials in solution,[2,3] $E°(VO_2^+/VO^{2+}) = 1$ V/NHE and $E°(MoO_2^{2+}/MoO^{3+}) = 0.48$ V/NHE, i.e., with the equation

$$V^VO_2^+ + Mo^VO^{3+} \rightarrow V^{IV}O^{2+} + Mo^{VI}O_2^{2+} \qquad (I)$$

Reactions at the solid−solid interface also show that V^V is more easily reducible than Mo^{VI}. Thus, during the preparation of $V_2O_5-MoO_3$ solid solutions by calcination of a mixture of salts or oxides at high temperature (700−1000 °C), part of the vanadium is reduced to the IV oxidation state as a result of charge compensation of the molybdenum ions.[4,5] When these solid solutions are partially reduced under vacuum at high temperature, only a V^{IV} signal is observed by EPR;[4,6] the absence of a Mo^V EPR signal was interpreted in terms of the stabilization of V^{IV} by Mo^{VI} in the mixed phase.[6]

One may wonder what reaction would develop at the gas−solid interface, using for instance $MoCl_5$ (Mo^V) as the gas-phase probe and V_2O_5 as the solid. Can we expect an electron transfer between Mo^V and V^V? In other words, can the redox potentials determined in solution be used to predict electron transfer at the gas−solid interface? To answer these questions, we chose to use silica-supported vanadium oxide as the solid rather that unsupported V_2O_5 to get a higher V_2O_5 surface area, and possibly point out different behaviors of surface V^V species.

Previous studies published by our group[7−10] showed that $MoCl_5$ could be grafted onto silica in air- and water-free conditions, via a reaction between $MoCl_5$ in the vapor phase at 200 °C and the hydroxyl groups of silica. It was shown by EPR and diffuse reflectance UV−vis−near-IR spectroscopies that two types of molybdenum species were deposited onto silica during the grafting reaction:[7−9]

(i) a monomeric grafted Mo^V species, $\equiv SiOMoCl_4$ ($g_\perp = 1.952$ and $g_\parallel = 1.968$), via the reaction

$$Mo^VCl_5 + \equiv SiOH \rightarrow \equiv SiOMo^VCl_4 + HCl \qquad (II)$$

and (ii) a physically adsorbed diamagnetic Mo_2Cl_{10} dimer.

So, another question may be addressed: would $MoCl_5$ react with V_2O_5 and/or silica?

If there is an electron transfer from Mo^V to V^V, it should be easily detected by EPR since the signals of Mo^V and V^{IV} are drastically different in shape, especially because their hyperfine structures are different (Table 1).

On the other hand, if $MoCl_5$ interacts with silica or V_2O_5 without electron transfer, the shape of the resulting Mo^V EPR

* Author to whom correspondence should be addressed. E-mail: louisc@ccr.jussieu.fr.
[†] Université Pierre et Marie Curie.
[‡] Université Paris VII-Denis Diderot.
[§] Institut Universitaire de France.

10.1021/jp022258c CCC: $25.00
Published on Web 08/28/2003

TABLE 1: Nuclear Magnetic Moment, Nuclear Spin, and Natural Abundance of Cations in Various Oxides[12]

oxide	nuclide	natural abundance (%)	nuclear spin	nuclear magnetic moment (μ_N)
MoO_3	^{95}Mo	15.9	5/2	−0.91
	^{97}Mo	9.6	5/2	−0.93
V_2O_5	^{51}V	99.8	7/2	5.15
Class 1[a]				
SiO_2	$^{28,30}Si$	95.3	0	
TiO_2	$^{46,48,50}Ti$	87.2	0	
ZrO_2	$^{90,92,94}Zr$	88.7	0	
Y_2O_3	^{89}Y	100.0	1/2	−0.14
Class 2[a]				
Al_2O_3	^{27}Al	100.0	5/2	3.64
Ga_2O_3	^{69}Ga	60.1	3/2	2.01
	^{71}Ga	39.9	3/2	2.56
La_2O_3	^{139}La	99.9	7/2	2.78

[a] According to the classification of oxides proposed by Cordischi et al.[11]

signal should enable us to determine with what compound $MoCl_5$ interacts. Indeed, according to Cordischi et al.,[11] the oxides can be classified into two classes (Table 1). Silica belongs to class 1, whereas vanadium ^{51}V, which has both a high nuclear spin and a high magnetic moment (Table 1), belongs to class 2. According to Cordischi et al.,[11] the interaction between Mo^V and silica (class 1) should be characterized by an EPR signal of Mo^V with its hyperfine structure whereas the interaction between Mo^V and V_2O_5 (class 2) should be characterized by an EPR signal of Mo^V with a superhyperfine structure due to the interaction of the unpaired electron spin of Mo^V with the nuclear spin of V^V.

Hence, the nature of the interaction between $MoCl_5$ and vanadium oxide or silica can be easily characterized whether there is an electron transfer or not.

Experimental Section

1. Sample Preparation. Silica Spherosil XOA 400 (S_{BET} = 500 $m^2 \cdot g^{-1}$, pore volume 1.25 $cm^3 \cdot g^{-1}$, average pore diameter ~80 Å, 4 ppm of Ca, and 60 ppm of Na) supplied by Rhône Poulenc (France) was used as a support.

A silica-supported vanadium sample (labeled V/SiO_2) with 10 wt % V was prepared by impregnation of silica with an aqueous solution of vanadyl oxalate (7.5 $mL \cdot g^{-1}$ of silica), obtained by dissolution of ammonium metavanadate (NH_4VO_3; Merck, 99% purity) in an aqueous solution of oxalic acid (60 $g \cdot L^{-1}$, Prolabo, 99.8% purity). The sample was dried in an oven at 60−70 °C for 1 h under continuous stirring and then at 80 °C for 5 h.

Before reaction with $MoCl_5$ (Merck, 99% purity), silica and V/SiO_2 were calcined to eliminate adsorbed water and avoid further $MoCl_5$ hydrolysis when $MoCl_5$ was introduced. In the case of V/SiO_2, calcination was also performed to decompose and oxidize the vanadyl oxalate (V^{IV}, paramagnetic) to vanadium oxide (V^V, diamagnetic). Calcination was performed at 450 °C (heating rate 10 °C·min^{-1}) for 15 h under oxygen (145 $mL \cdot min^{-1}$) in a flow reactor equipped with a side arm EPR tube. Silica was then treated at 450 °C for 15 min under flowing argon, whereas the V/SiO_2 sample was cooled to room temperature under flowing oxygen and evacuated for 5 min. Even with a short evacuation time, it was impossible to completely avoid the formation of V^{IV} ions. Afterward, these samples were transferred into the side arm EPR tube, which was sealed under vacuum.

The same procedure of grafting in the vapor phase as that described in ref 8 was used for the reaction of $MoCl_5$ with silica and V/SiO_2, but at 30 instead of 200 °C. Indeed, it was observed that the intensity of the V^{IV} signal decreased at 200 °C under static vacuum and could interfere with the evolution of the V^{IV} signal during the reaction with $MoCl_5$. To follow this reaction by EPR, an EPR tube containing about 20 mg of silica or V/SiO_2 was connected to a glass ampule containing about 1 g of $MoCl_5$ (black solid Mo_2Cl_{10}) under static vacuum. The tube and the ampule were separated from each other by a stopcock. A cell for diffuse reflectance UV−vis−near-IR spectroscopy was also added to the EPR tube.

During reaction with $MoCl_5$ at 30 °C, the samples were characterized by these two techniques, and the SiO_2 and V/SiO_2 samples were labeled as Mo/SiO_2 and $Mo-V/SiO_2$, respectively. It may be noted that the reaction with the V/SiO_2 sample was very slow, and was therefore followed during a very long period of time up to 9000 h.

The vapor pressures of $MoCl_5$ and Cl_2 (arising from the reaction $2MoCl_5(s) \rightarrow 2MoCl_4(s) + Cl_2(g)$) at 30 °C were equal to $\sim 10^{-2}$ and $\sim 10^{-4}$ Torr, respectively, on the basis of the equations proposed by Saeki et al.[13]

2. Techniques. The chemical analyses of the samples were performed by inductive coupling plasma at the CNRS Center of Chemical Analysis (Vernaison, France). In the following, the V and Mo weight loadings of the samples are expressed in weight percent for samples calcined in air at 1000 °C:

$$\text{wt \% V} = M_V/(M_{V_2O_5} + M_{SiO_2}) \times 100, \text{ and}$$

$$\text{wt \% Mo} = M_{Mo}/(M_{MoO_3} + M_{V_2O_5} + M_{SiO_2}) \times 100$$

The EPR spectra were recorded at 77 K for various times of reaction on a Bruker ESP300E spectrometer operating at 9.23 GHz (X band) with a field modulation of 100 kHz, an amplitude modulation of 10 G (10^4 G = 1 T), and a microwave power of 10 mW. Before the spectra were recorded, $MoCl_5$ of the gas phase was condensed by liquid nitrogen trapping in the side arm tube containing solid $MoCl_5$. After double integration of the spectra, the concentration of the V^{IV} spins was estimated thanks to a standard curve of the double integration of the V^{IV} signal of vanadyl sulfate in aqueous solution versus concentration. It was checked that the use of this standard in solution is valid for the determination of the spin concentration of solid samples: a sample of known concentration of vanadyl sulfate diluted in a solid diamagnetic matrix of K_2SO_4, supplied by Dyrek et al.,[14,15] gave a signal whose double integration value lies on the standard curve. The estimated error was about 5%. The same standard curve was used to estimate the Mo^V spin concentration. This is justified because Mo^V and V^{IV} have the same d^1 electronic configuration and the same S value (S = 1/2).[16] The EPR parameters of the V^{IV} and Mo^V signals were determined after simulation and adjustment of the calculated EPR spectrum with the experimental one, with the software SIM14DOS,[17] using successively the Grid Search and Simplex methods.

Diffuse reflectance UV−vis−near-IR spectra were recorded in the range 230−2500 nm with a 5270 Beckman spectrometer equipped with an integration sphere and a double monochromator. $BaSO_4$ was used as a reference. Diffuse reflectance spectra were recorded in air-free conditions.

XPS spectra were recorded at room temperature under ultrahigh vacuum (10^{-9} Torr) on a Surface Science Instruments SSX100 spectrometer. The samples were impinged by a

monochromated beam of X photons coming from the Kα emission of an Al anode ($h\nu = 1486.6$ eV). The width of the X photon beam was 600 μm. The pass energy was 50 eV (resolution <1 eV). The powder samples were transferred with no contact with air from the reactor into a glass tube, which was sealed under vacuum. Then, the glass tube was broken in an inflatable glovebag attached to the introduction chamber of the spectrometer, and the sample was transferred in the latter under an argon stream, and evacuated overnight. The negative charge, created by the electron beam on the silica surface, could not spread over the silica surface because of the insulating character of silica and may induce the deformation of the XPS peaks. A charge compensation low-energy electron beam was applied to eliminate this effect. The binding energy of all the ions was normalized to the Si 2p peak located at 103.4 eV, used as an internal reference. The acquisition step was 0.1 eV, and the reproducibility of the binding energy measurements was on the order of 0.25 eV, quite smaller than the observed chemical shifts of the V 2p or Mo 3d lines. The use of a monochromated Al source ensured no superposition of O 1s satellite lines and V 2p peaks. The peak fitting was performed using the manufacturer's (Surface Science Instruments) software: after subtraction of a Shirley baseline, Gaussian−Lorentzian peaks were used to fit the signal with a standard least-squares routine, using as much as possible similar widths when several lines were present. The peak areas were measured and the atomic percentages were calculated by taking into account Scofield's cross sections[18] and the $E_{\text{kinetics}}^{1/2}$ dependence of the mean free paths of electrons. In fact, the mean free paths also depend on the solid studied. As a consequence, for our silica-supported V−Mo samples, the Mo/V atomic ratios calculated from the atomic percentages could not be considered as quantitative and compared to those obtained from chemical analysis. The Mo or V peaks were adjusted using the following conditions: (i) the Mo $3d_{5/2}$ and $3d_{3/2}$ peaks are separated by 3.1 eV, and their intensity ratio $Mo3d_{5/2}/Mo3d_{3/2} = 3/2$; (ii) the V $2p_{3/2}$ and $2p_{1/2}$ peaks are separated by 7.5 eV, and their intensity ratio $V2p_{3/2}/V2p_{1/2} = 2$; (iii) these peaks were assumed to be 90% Gaussian and 10% Lorentzian. Since the difference in energy between the Mo $3d_{5/2}$ and $3d_{3/2}$ peaks, and between the V $2p_{3/2}$ and $2p_{1/2}$ peaks, is constant, only the positions of the Mo $3d_{5/2}$ and the V $2p_{3/2}$ peaks will be discussed in the following.

Raman scattering was excited using the 514.5 nm line from an Ar^+ laser (Spectra-Physics model 165). The Raman spectra were recorded at room temperature on a multichannel Dilor XY modular spectrometer. This apparatus consisted of a double monochromator used in subtrative mode (i.e., with no dispersion), followed by a spectrograph and an intensified 1024 diode-array detector cooled by the Peltier effect. The samples were irradiated using a 180° configuration (retro-Raman). Low laser power (20−50 mW) and a rotating system were used to avoid any thermal or photochemical decomposition. With the most commonly used slit (100 μm), the spectral resolution was estimated to be ~4 cm^{-1}. Before the Raman spectra were recorded, the powder samples were transferred in air-free conditions, from the reactor into a quartz tube, which was sealed afterwards.

STEM studies and EDX analyses were performed with a JEOL JEM 100CXII microscope equipped with a scanning device, ASID 4D, and using a Link AN10000 system connected to a silicon−lithium diode detector and a multichannel analyzer.

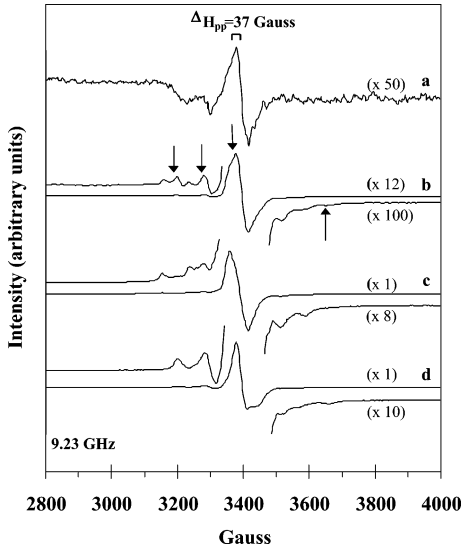

Figure 1. In situ EPR spectra (X-band) of Mo/SiO_2 samples recorded at 77 K after different times of reaction of $MoCl_5$ with silica at 30 °C: (a) 2 h; (b) 88 h (the same spectrum up to 1000 h) (signals **MS1** and **MS2**); (c) 1230 h (signal **MS1**); (d) signal **MS2** obtained by subtraction of spectrum c from spectrum b.

Results

1. Chemical Analysis. The Mo loading of Mo/SiO_2 is 0.6 wt % after 3600 h of reaction, while the Mo and V loadings of $Mo-V/SiO_2$ are 4.5 and 9.1 wt %, respectively, after 4500 h of reaction.

To eliminate the Mo species which are physisorbed or weakly bonded to the surface of the sample as in the case of grafting of $MoCl_5$ on silica at 200 °C,[8] $Mo-V/SiO_2$ was washed in bidistilled water (10 $mL \cdot g^{-1}$) under magnetic stirring for 5 min at room temperature. After washing and drying, the Mo and V loadings are weaker: 0.44 and 0.98 wt %, respectively. It is noted that the V/Mo atomic ratio is equal to ~4 whether $Mo-V/SiO_2$ is washed or not.

2. EPR Spectroscopy. *a. Reaction of $MoCl_5$ with Silica at 30 °C.* After calcination, silica is white and no EPR signal is observed. After 2 h of reaction of $MoCl_5$ with silica at 30 °C, the sample becomes pale yellow and a Mo^V EPR signal is observed (Figure 1a). After about 90 h of reaction, the hyperfine structure of the Mo^V signal starts to be visible (Figure 1b). The spectrum shape and the sample color remain unchanged up to 1000 h of reaction (Figure 1b) although the intensity of the EPR signal gradually increases up to 1×10^{18} spins$\cdot g^{-1}$ (Figure 2).

Beyond 1000 h of reaction, the sample becomes orange and the signal intensity decreases (Figure 2). The EPR signal, labeled **MS1**, is now different (Figure 1c) since the four lines indicated by arrows in Figure 1b are not observed any further. The best fit of spectrum **MS1** corresponds to the following EPR parameters: $g_\perp = 1.944$, $g_\parallel = 1.960$, $a_\perp = 43$ G, $a_\parallel = 86$ G. Hence, the spectrum observed below 1000 h of reaction (Figure 1b) results from the superimposition of at least two signals: signal **MS1** and another one labeled **MS2**. The latter (Figure 1d) can be extracted by subtracting signal **MS1** from the spectrum obtained after 88 h (Figure 1b). The EPR parameters obtained for the best fit of signal **MS2** are $g_\perp = 1.950$, $g_\parallel = 1.918$, $a_\perp = 39$ G, and $a_\parallel = 100$ G.

b. Reaction of $MoCl_5$ with V/SiO_2 at 30 °C. The evolution of the intensity of the EPR spectrum observed during the reaction of V/SiO_2 with $MoCl_5$ at 30 °C can be decomposed into four main stages, on the basis of the changes of sample color, which

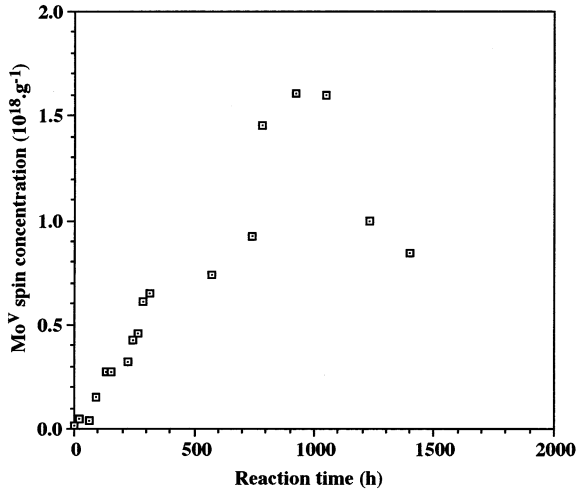

Figure 2. Changes in the Mo^V spin concentration versus the time of reaction of $MoCl_5$ with silica at 30 °C.

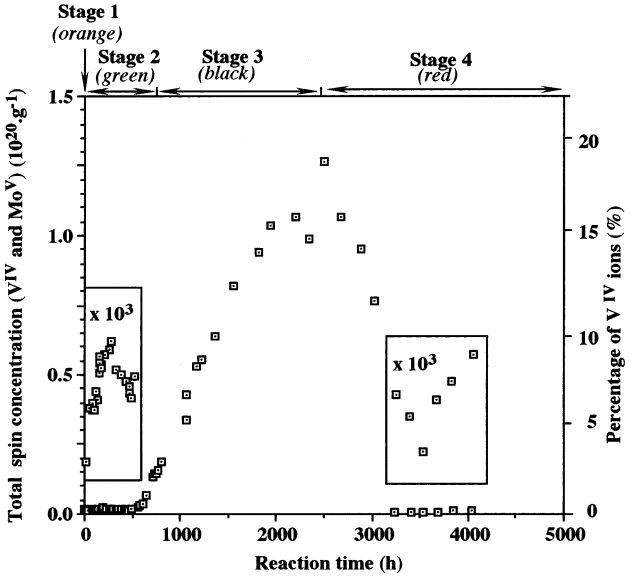

Figure 3. Changes in the spin concentration versus the time of reaction of $MoCl_5$ with V/SiO_2 at 30 °C.

are associated with changes in spin concentration and EPR signal (Figure 3). The EPR spectra are reported in Figure 4 and the results summarized in Table 2.

The four stages can be described as follows.

Stage 1 (orange sample, 0−20 h): The EPR spectrum of V/SiO_2 after calcination and within the first ∼20 h of reaction does not change in shape and in intensity (1×10^{18} spins·g^{-1}). It exhibits the same broad symmetric and structureless signal **VS1** (peak to peak line width, $\Delta H_{pp} \approx 100$ G) centered at $g_{iso} = 1.968$ (Figure 4a). The signal is attributed to magnetically interacting V^{IV} ions.[19]

Stage 2 (green sample, 20−500 h): Between ∼20 and ∼300 h of reaction (Figure 4b), the spectrum intensity remains weak, but a signal of magnetically isolated V^{IV} ions labeled **VS2** appears, superimposed on signal **VS1**. The parameters of signal **VS2** obtained by simulation are $g_\perp = 1.985$, $g_\parallel = 1.905$, $a_\perp = 79$ G, and $a_\parallel = 188$ G, which indicate that these V^{IV} ions are in axial symmetry. The V^{IV} spin concentration increases from 1×10^{18} to 2×10^{18} spins·g^{-1} up to ∼300 h of reaction, which corresponds to about 0.3% of the overall V ions (Figure 3). However, between 300 and ∼500 h of reaction, the signal decreases to 1.5×10^{18} spins·g^{-1} (0.2% of the overall V ions),

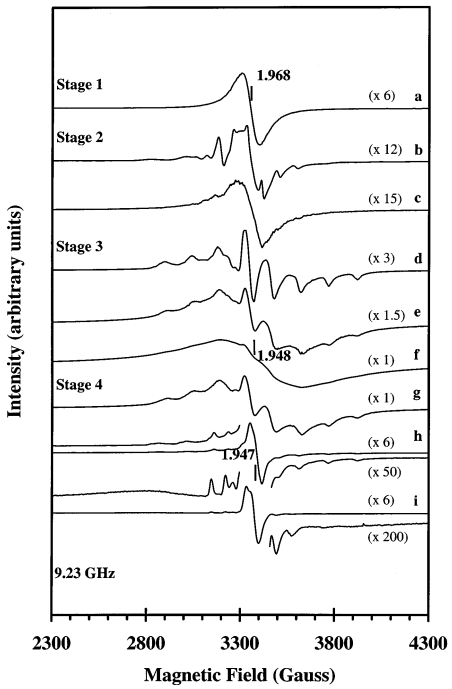

Figure 4. In situ EPR spectra (X-band) of $Mo-V/SiO_2$ samples recorded at 77 K after different times of reaction of $MoCl_5$ with V/SiO_2 at 30 °C: (a) 0−20 h; (b) 86 h; (c) 450 h; (d) 700 h; (e) 1400 h; (f) 2500 h; (g) 3000 h; (h) 3200 h; (i) 8800 h.

the hyperfine structure tends to disappear (Figure 4c), and only signal **VS1** remains visible.

Stage 3 (black sample, 500−2500 h): Between ∼500 and ∼800 h of reaction, a new signal of V^{IV} ions with a hyperfine structure appears (Figure 4d), and the sample turns black. It results from the contribution of two signals whose respective EPR parameters were obtained by simulation, (i) a signal labeled **VS3** of magnetically isolated V^{IV} ions in axial symmetry, $g_\perp = 1.941$, $g_\parallel = 1.936$, $a_\perp = 13$ G, $a_\parallel = 147$ G, whose intensity corresponds to 30% of the spectrum intensity and (ii) a broad signal labeled **VS4** of magnetically interacting V^{IV} ions, $g_{iso} = 1.948$, $\Delta H_{pp} \approx 500$ G, corresponding to 70% of the spectrum intensity. We checked that no V^{III} EPR signal was detected at 4 K.

Between ∼1000 and ∼2500 h of reaction, signal **VS3** gradually disappears (Figure 4e,f), and only signal **VS4** remains visible.

The overall spectrum drastically increases in intensity during stage 3 from 1.7×10^{18} to 1.3×10^{20} spins·g^{-1} (Figure 3), which corresponds to an increase from 0.2% to 20% of the overall V ions.

Stage 4 (red sample, 2500−9000 h): between ∼2500 and ∼3000 h of reaction, the sample is dark red and signal **VS3** appears again, superimposed on a broad signal, **VS4′**, of V^{IV} ions (Figure 4g). The overall spectrum drastically decreases in intensity from 1.3×10^{20} to 5.6×10^{17} spins·g^{-1}, which corresponds to a decrease from 20% to 0.1% of the V ions, i.e., to a percentage of V^{IV} ions as small as in stages 1 and 2 (Figure 3).

Beyond ∼3200 h of reaction, the sample turns red and an asymmetric signal of Mo^V ions (**MS3**, $g_{iso} = 1.947$, $\Delta H_{pp} = 50$ G) appears surrounded by several weak lines of signal **VS3** (Figure 4h). The Mo^V signal increases in intensity and becomes predominant. The overall spectrum slightly increases in intensity from 5.6×10^{17} to 1.0×10^{18} spins·g^{-1} (Figure 3). After ∼8800 h (Figure 4i), the sample is still red, signal **VS3** has disappeared,

TABLE 2: EPR Results Obtained during the Various Stages of Reaction between $MoCl_5$ and V/SiO_2 at 30 °C

reaction stage and sample color	reaction time (h)	signal[a]	EPR parameters $g_\perp$	$g_\parallel$	g_{iso}	$a_\perp$ (G)	$a_\parallel$ (G)	ΔH_{pp} (G)	percentage of spin[b]
stage 1	0−20	**VS1**			1.968			100	0.2%
orange sample									
stage 2	20−500	**VS1**			1.968			100	increase from 0.2% to 0.3% (∼300 h) and
green sample		**VS2**	1.985	1.905	1.958	79	188		then decrease from 0.3% to 0.2%
stage 3	500−800	**VS3**	1.941	1.936		13	147		increase from 0.2% to ∼20%
black sample		**VS4**			1.948			500	
	1000−2500	**VS4**			1.948			500	
stage 4	2500−3000	**VS3**	1.941	1.930		13	150		decrease from 20% to 0.1%
dark red sample		**VS4′**			1.934			600	
red sample	∼3200	**VS3**	1.941	1.930		13	150		
		MS3			1.947			50	
	>8800	**VS4″**			1.94			800	increase from 0.1% to 0.6%
		MS3			1.947			50	

[a] **VS** = V^{IV} signal; **MS** = Mo^V signal. [b] Ratio of the spin number obtained from the double integration of the EPR spectra (V^{IV} and possibly Mo^V) over the total V ion number.

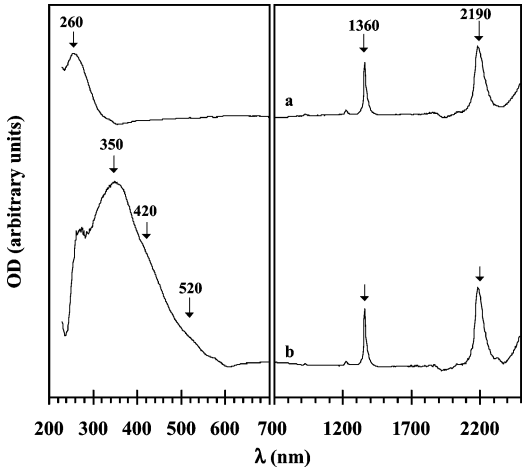

Figure 5. In situ diffuse reflectance UV−vis−near-IR spectra recorded at room temperature of (a) SiO_2 after calcination at 450 °C and (b) Mo/SiO_2 (960 h).

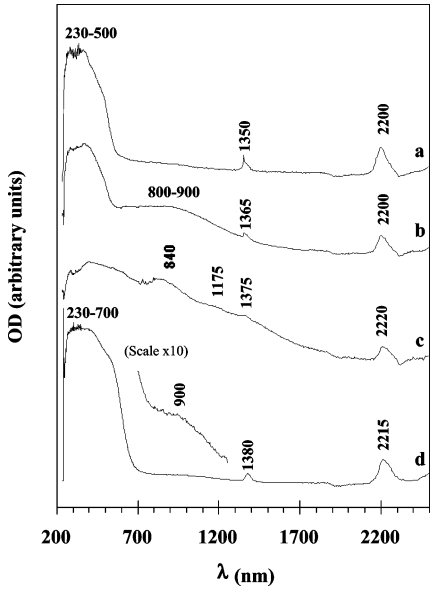

Figure 6. In situ diffuse reflectance UV−vis−near-IR spectra of Mo−V/SiO_2 recorded at room temperature after different times of reaction of V/SiO_2 with $MoCl_5$ at 30 °C: (a) 0−20 h (stage 1); (b) 48 h (stage 2); (c) 890 h (stage 3); (d) 8800 h (stage 4).

the Mo^V signal **MS3** is the main signal, but a weak and broad signal, **VS4″**, of V^{IV} ions is visible (ΔH_{pp} = 800 G).

3. Diffuse Reflectance UV−Vis−Near-IR Spectroscopy. *a. Reaction of $MoCl_5$ with Silica at 30 °C.* The UV−vis−near-IR spectrum of silica after calcination (Figure 5a) exhibits three bands: an absorption band at 260 nm corresponding to the $O^{2-} \rightarrow Si^{4+}$ ligand−metal charge-transfer (LMCT) band and two narrow bands at 1360 and 2190 nm. The first one corresponds to the first harmonic 2ν of the stretching vibration of free surface hydroxyl groups and the second one to the combination ($\nu + \delta$) of the stretching and the bending vibration modes.[20]

After ∼960 h of reaction of $MoCl_5$ with silica at 30 °C, new absorption bands appear, superimposed on the previous ones: a broad one at 350 nm with weak shoulders at 420 and 520 nm (Figure 5b). The intensity of the bands at 1360 and 2190 nm remains constant.

b. Reaction of $MoCl_5$ with V/SiO_2 at 30 °C. The UV−vis−near-IR spectra of V/SiO_2 do not change during the first 20 h of reaction (stage 1, orange) with $MoCl_5$ at 30 °C (Figure 6a). They exhibit the two narrow bands at 1350 and 2200 nm already observed on silica (Figure 5a) and a broader charge-transfer band between 230 and 500 nm (with maxima at 300 and 400 nm and shoulders at ∼440 and 500 nm) than with silica (Figure 5a) because of the additional $O^{2-} \rightarrow V^{5+}$ LMCT bands. During stage 2 (green, 20−500 h), a broad band appears with a maximum at 800−900 nm (Figure 6b). During stage 3 (black, 500−800 h), the intensity of this band increases, the LMCT band broadens, and an additional shoulder becomes visible at ∼1175 nm (Figure 6c). During stage 4 (red, 2500−8800 h), the broad bands between 600 and 2000 nm disappear, and the LMCT band is broader (Figure 6d) than that observed before reaction (Figure 6a): a shoulder is visible at 550 nm. During these four stages, the intensities of the bands at 1350 and 2200 nm decreased and the band at 1350 nm gradually shifted toward higher wavelength (1380 nm).

4. X-ray Photoelectron Spectroscopy. *a. Reaction of $MoCl_5$ with Silica*. The binding energy of the XPS peaks observed on silica before reaction (O and Si components) and after 3400 h of reaction with $MoCl_5$ at 30 °C (Mo, Cl, O, and Si components) and their corresponding atomic percentages are reported in Table 3. On Mo/SiO_2 (3400 h), new very weak peaks appear: the Mo $3d_{5/2}$ peak at 230.7 eV, characteristic of Mo^V ions,[21−23] and the Cl 2p peak at 200.7 eV (the two Cl $2p_{3/2}$ and $2p_{1/2}$ peaks are too weak to be distinguishable).

b. Reaction of $MoCl_5$ with V/SiO_2. V/SiO_2 exhibits an XPS V $2p_{3/2}$ peak at 518.1 eV, characteristic of V^V ions surrounded

TABLE 3: Binding Energies (BE) and Atomic Percentages of the Elements in SiO_2 and V/SiO_2, before and after Reaction with $MoCl_5$ at 30 °C (without Contact with Air)[a]

sample		V $2p_{3/2}$	Mo $3d_{5/2}$	Cl 2p	O 1s	Si 2p
SiO_2	BE (eV)				532.8	103.4
	atomic %				70.0	27.4
Mo/SiO_2 (3400 h)	BE (eV)		230.7	200.7	532.7	103.4
	atomic %		0.2	0.6	68.3	28.1
V/SiO_2	BE (eV)	518.1			531.1, 532.5	103.4
	atomic %	4.4			65.0	22.7
$Mo-V/SiO_2$, stage 4 (8800 h)	BE (eV)	517.0	232.6	199.1, 200.9	530.9, 532.6	103.4
	atomic %	5.7	3.5	10.8, 3.1	51.4	13.7

[a] The atomic percentage of element X is expressed as the ratio of the XPS peak area of X to the sum of the peak areas of all the elements. Because of the presence of carbon on SiO_2 and V/SiO_2 (BE ≈ 285 and 287 eV), the sum of the atomic percentages mentioned in this table is lower than 100.

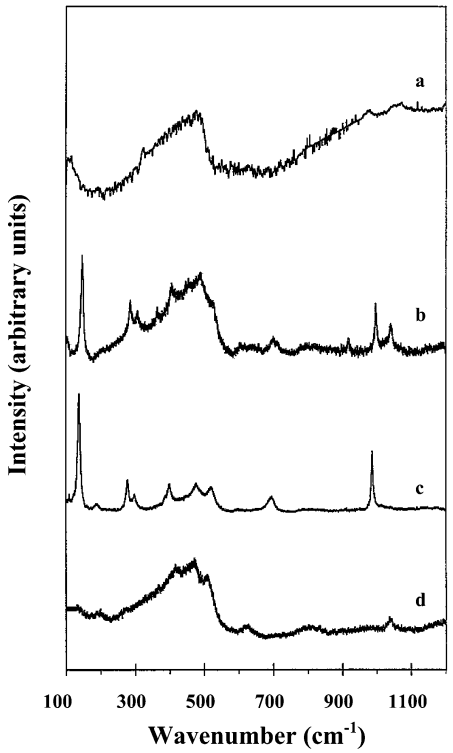

Figure 7. In situ Raman spectra, recorded at room temperature, of (a) SiO_2 after calcination at 450 °C, (b) V/SiO_2 after calcination at 450 °C, (c) bulk V_2O_5, and (d) $Mo-V/SiO_2$ (stage 4, 8800 h).

by oxygen ligands.[23] The O 1s peak at 532.4 eV is the envelope of two peaks, the main one at 532.5 eV attributed to oxygen of silica[23] and the minor one at ~531.1 eV to oxygen bonded to vanadium.[24]

After reaction with $MoCl_5$ (stage 4, 8800 h), new XPS peaks of Mo $3d_{3/2}$ and $3d_{5/2}$ and two Cl $2p_{3/2}$ and $2p_{1/2}$ peaks at 199.1 and 200.9 eV are visible. The binding energy of Mo $3d_{5/2}$ (232.6 eV) (Table 3) is higher than that of Mo^V supported on silica (230.7 eV), and may be attributed to Mo^{VI} ions.[23] In addition, the binding energy of V $2p_{3/2}$ shifts from 518.1 eV on V/SiO_2 to 517.0 eV on $Mo-V/SiO_2$ (stage 4), which indicates the reduction of V^V ions to V^{IV}. Indeed, a decrease of 1 eV in binding energy is usually observed for the reduction of V^V to V^{IV}.[24] The binding energies of the two O 1s peaks observed on V/SiO_2 do not change significantly during reaction with $MoCl_5$.

5. Raman Spectroscopy. The spectrum obtained after reaction of $MoCl_5$ with silica was too weak and noisy to be exploitable. Comparison of the Raman spectrum of V/SiO_2 (Figure 7b) with those of SiO_2 (Figure 7a) and V_2O_5 (Figure 7c) shows that V/SiO_2 contains V_2O_5 crystallites. The vibration line assignments are reported in Table 4. According to Le Coustumer et al.[25] and Oyama et al.,[26] the line at 1038 cm^{-1} can be attributed to the V═O stretching vibration of a monomeric vanadyl species in tetrahedral coordination bonded to silica ($(\equiv SiO)_3V{=}O$).

The Raman spectrum of $Mo-V/SiO_2$ (stage 4, 8800 h) is shown in Figure 7d. The bands characteristic of V_2O_5 have disappeared, while that at 1038 cm^{-1} attributed to monomeric vanadyl species remains visible. The bands of the deformation modes of the Si−O−Si bonds at 492, 456, and 398 cm^{-1},[28−33] which were hidden by those of V_2O_5, are now visible. The band at 804 cm^{-1} may be assigned to the symmetric stretching vibration of Si−O−Si bonds, which is usually observed at 800 cm^{-1},[28−33] or to the Mo−O asymmetric stretching, which was observed at ~800 cm^{-1} in a mixed oxide containing 95% V_2O_5 and 5% MoO_3.[34]

6. Electron Microscopy. Scanning transmission electron microscopy (STEM) of V/SiO_2 reveals the presence of rod-shaped V_2O_5 microcrystallites in interaction or not with silica. The lengths of the rods are in the range 100−600 nm with a 10−50 nm width. In addition, in areas of bare silica, EDX shows the presence of vanadium. The $Mo-V/SiO_2$ sample (stage 4, 8800 h and after contact with air) no longer exhibits V_2O_5 crystallites observed by STEM.

Discussion

Before the evolution of the V/SiO_2 sample during the reaction with $MoCl_5$ at 30 °C is analyzed, the results obtained with SiO_2 are first discussed.

1. Reaction of $MoCl_5$ with Silica at 30 °C. *a. Reaction beyond 1000 h.* For the sake of convenience, the results obtained after 1000 h of reaction of $MoCl_5$ with silica at 30 °C are first examined. The sample exhibits an EPR signal, **MS1** (Figure 1c), whose parameters ($g_\perp = 1.944$, $g_\parallel = 1.960$, $a_\perp = 43$ G, $a_\parallel = 86$ G) are slightly different from those obtained after reaction at 200 °C ($g_\perp = 1.952$, $g_\parallel = 1.968$, $a_\perp = 44$ G, $a_\parallel = 82$ G), which were attributed to $\equiv SiOMoCl_4$ species grafted onto silica.[8] It is noted that $g_\perp$ is lower than $g_\parallel$ in both cases, which indicates that the Mo^V ions are still surrounded by Cl ligands.[35] This is confirmed by the presence of the Cl 2p peak at 200.7 eV in the XPS spectrum. It may be noted that HCl formed during reaction II cannot react with the silica surface at this temperature, but only above 300 °C.[36]

The intensities of the OH vibration bands of silica at 1360 and 2190 nm do not change during the reaction of $MoCl_5$ with SiO_2 at 30 °C (Figure 5b), while they decreased during the reaction at 200 °C.[8] This can be due to the much lower Mo loading on silica at 30 °C (0.6 wt % after 3600 h) than at 200 °C (6.2 wt %).[8] The UV−vis absorption bands after reaction at 30 °C (Figure 5b) are also different from those observed after reaction at 200 °C, which were attributed to $MoOCl_4^-$ by

TABLE 4: Location and Assignment of the Raman Bands Observed on V/SiO_2, before and after Reaction with $MoCl_5$ at 30 °C (Stage 4, 8800 h) (without Contact with Air)

sample	Raman bands (cm^{-1})	vibration mode	symmetry/structure	ref
V/SiO_2	1038	V═O symmetric stretching	monomeric vanadyl species	25, 26
	993	V═O symmetric stretching	octahedron in decavanadate $V_{10}O_{28}^{6-}$	27
	703	V−O−V asymmetric bending	distorted octahedron in V_2O_5 microcrystallites	25, 27
	602	V−O−V symmetric bending	distorted octahedron in V_2O_5 microcrystallites	25, 27
	525, 477, 402, 302, 283, 195, 144	V−O−V bending	distorted octahedron in V_2O_5	27
$Mo-V/SiO_2$ (stage 4, 8800 h)	1038	V═O symmetric stretching	monomeric vanadyl species bonded to silica	25, 26
	804	Si−O−Si symmetric stretching or Mo−O asymmetric stretching	SiO_2 mixed $V_2O_5-MoO_3$	28−31 32−34
	492, 456, 358	Si−O−Si bending	SiO_2	28−33

TABLE 5: UV−Vis Bands of Mo/SiO_2 Samples Obtained after Reaction of SiO_2 with $MoCl_5$ at 30 and 200 °C and of Reference Chloride Compounds Containing Mo^V Ions[a]

sample	Mo/SiO_2 30 °C	Mo/SiO_2 200 °C	$MoCl_5$ in N_2 matrix	$MoOCl_4$ in N_2 matrix	$(MoOCl_4)^-$ in $AsPh_4MoOCl_4$	$(MoOCl_5)^{2-}$ in $(NH_4)_2MoOCl_5$
ref	this work	7	37	38	39	40
λ (nm)	350	365	CT: 345	340	380	375
	420 (sh)	460 (sh)	385	480	445	435
	520	625 (sh)	d−d: 460	635(w) 650 (w)	650	725

[a] sh = shoulder; w = weak.

comparison with model compounds (Table 5). It may be noted that they are also different from those of $MoCl_5$ (Table 5).

From all these results, it is concluded that the Mo^V ions present on the silica surface are surrounded by chlorine ions. It is not clear whether they have reacted with the silica surface since their EPR and UV−vis parameters are slightly different from those attributed to ≡$SiOMoCl_4$ species and from those of $MoCl_5$. They are assigned to $MoCl_5$ adsorbed on SiO_2 (species **MS1**, labeled $SiOH\cdots MoCl_5$).

b. Reaction below 1000 h. Below 1000 h of reaction of $MoCl_5$ with SiO_2 at 30 °C, the Mo^V EPR spectrum (Figure 1b) results from the superimposition of two signals, **MS1** and **MS2**. The relative values of the *g* components of signal **MS2** ($g_\perp$ (1.950) > $g_{||}$ (1.918)) are reversed with respect to those of signal **MS1** ($g_\perp$ (1.944) < $g_{||}$ (1.960)). Such an inversion of the *g* components is characteristic of the replacement of chlorine by surface oxygen ligands in molybdenyl species.[35] It is due to the fact that the spin−orbit coupling constant (λ_L) of the atoms bonded to Mo is present only in the expression of $g_{||}$. It drastically decreases when Cl ligands (λ_L = 587 cm^{-1}) are replaced by oxygen ligands (λ_L = 152 cm^{-1}), which induces a decrease in the $g_{||}$ value. It is noted that signal **MS2** was not observed during reaction of $MoCl_5$ with SiO_2 at 200 °C.[7,8] Since the experiment at 30 °C expands over a long period of time, it is likely that the silanol groups, which are around the Mo^V ions or which can migrate on the silica surface,[41,42] can hydrolyze the Mo−Cl bonds, according to the following reactions:

$$2\,{\equiv}Si{-}OH + SiOH\cdots Mo^{V}Cl_5 \rightarrow {\equiv}Si{-}O{-}Si{\equiv} + SiOH\cdots Mo^{V}(OH)Cl_4 + HCl \quad \text{(III)}$$

$$2\,{\equiv}Si{-}OH + SiOH\cdots Mo^{V}(OH)Cl_4 \rightarrow {\equiv}Si{-}O{-}Si{\equiv} + SiOH\cdots Mo^{V}(OH)_2Cl_3 + HCl \quad \text{(IV)}$$

Hence, signal **MS2** can be tentatively attributed to a hydrolyzed adsorbed Mo^V species, labeled $SiOH\cdots Mo^V(OH)_xCl_{5-x}$ with $1 \le x \le 5$.

Between 1000 and 1500 h of reaction, the Mo^V spin concentration decreases by 50% (Figure 2), and signal **MS2** disappears, leaving only signal **MS1** visible (Figure 1c). Contributions of **MS1** and **MS2** to the EPR spectra recorded below 1000 h of reaction can be obtained by deconvolution and double integration. Since the contribution of signal **MS2** to the EPR spectrum (1000 h of reaction) is 16%, the 50% decrease in the Mo^V spin concentration between 1000 and 1500 h of reaction (Figure 2) can be attributed not only to the disappearance of signal **MS2** but also to the decrease of signal **MS1**. Since the oxidation of Mo^V to Mo^{VI} ions can be ruled out because only Mo^V ions are detected by XPS (230.7 eV) (Table 3), it is proposed that a reaction between $MoCl_5$ and one hydroxyl group of species **MS2** occurs

$$MoCl_5 + Mo^{V}(OH)_xCl_{5-x} \rightarrow SiOH\ldots Mo^{V}(OH)_{x-1}\text{-}O\text{-}Mo^{V}\text{-}Cl_4 + HCl \quad \text{(V)}$$
(with Cl_{5-x} on the second Mo)

and leads to the formation of Mo^V-O-Mo^V dimers. Although no EPR signal was observed at half magnetic field, which might indicate their formation, this does not mean that Mo^V pairs are not formed. Indeed, they are difficult to observe on oxide surfaces[43] because of strong magnetic coupling[44] or inhomogeneity of the surface sites.[45] Hence, the decrease in signal **MS1** is tentatively attributed to the gradual hydrolysis of the molybdenum(V) chloride species (species **MS1**) to species **MS2** (reactions III and IV); then, the reaction between species **MS2** and $MoCl_5$ could lead to the formation of adsorbed Mo^V-O-Mo^V dimers (reaction V). The decrease in the Mo^V spin concentration suggests that reaction V is faster than reactions III and IV.

This interpretation is consistent with the following data: (i) molybdenum ions are in the V oxidation state, according to the XPS results; (ii) the Mo loading is 0.6 wt % after 4000 h of reaction, whereas the Mo^V ions visible by EPR correspond to a Mo loading of only ~0.01 wt %.

2. Evolution of V/SiO_2 during the Reaction with $MoCl_5$ at 30 °C. *a. Starting V/SiO_2.* According to the Raman spectrum (Figure 7b and Table 4), V/SiO_2 before reaction contains monomeric vanadyl species, $(\equiv SiO)_3V{=}O$ and V_2O_5 crystallites. This result is consistent with the observation of V_2O_5 microcrystallites supported or not on silica by STEM, and the

detection of vanadium by EDX in areas of bare silica support. The absorption bands in the 300−500 nm range (Figure 6a) correspond to the $O^{2-} \rightarrow V^{5+}$ LMCT bands in V_2O_5.[46,47] According to the XPS results, the vanadium ions are in the V oxidation state. However, the broad EPR signal **VS1** (Figure 4a) indicates the presence of magnetically interacting V^{IV} ions. It corresponds to about 0.2% of the overall V ions (Figure 3). The V^{IV} EPR signal indicates that it is not possible to avoid the reduction of V^V ions even when the oxygen gas phase is eliminated fast at room temperature after calcination. This reduction probably only occurs on the surface of the V_2O_5 crystallites since it was checked that an adsorption of O_2 at low pressure and room temperature induces a decrease and broadening of this V^{IV} signal.

b. Mo−V/SiO₂ at Stage 4 of the Reaction. For the sake of convenience, the results obtained during stage 4 of the reaction are first examined. When gaseous $MoCl_5$ is put into contact with V/SiO_2 at 30 °C, a reaction between $MoCl_5$ and vanadium oxide occurs, as attested by the higher Mo loading in $Mo-V/SiO_2$ (4.5 wt % after 4500 h) than in Mo/SiO_2 (0.6 wt % after 4000 h).

The monomeric vanadyl species does not significantly react with $MoCl_5$ since the associated Raman band at 1038 cm^{-1} (Figure 7d) is still present after reaction. However, the disappearance of the V_2O_5 microcrystallites observed by STEM and of the associated Raman bands (Figure 7d) indicates that $MoCl_5$ deeply alters the structure of V_2O_5, which transforms into an amorphous phase. It is well-known that an amorphous phase exhibits a weaker Raman scattering cross section than a crystallized phase, which explains why a new amorphous phase is not detected by Raman spectroscopy.

The XPS results show that molybdenum is in the VI oxidation state, which was not observed during the reaction between $MoCl_5$ and silica (Table 3), and that there is a shift in the binding energy of V from 518.1 to 517.0 eV (Table 3), indicating the reduction of V^V to V^{IV} on the basis of earlier work.[24] The presence of V^{IV} and Mo^{VI} ions after reaction suggests that an electron transfer from Mo^V to V^V occurs when $MoCl_5$ reacts with supported V_2O_5:

$$Mo^V + V^V \rightarrow Mo^{VI} + V^{IV} \qquad \text{(VI)}$$

This electron transfer is consistent with the prediction given by the redox potentials of the VO_2^+/VO^{2+} and MoO_2^{2+}/MoO^{3+} couples in solution, 1 and 0.48 V/NHE, respectively[2,3] (eq I).

Two Cl $2p_{3/2}$ and $2p_{1/2}$ peaks at 199.1 and 200.9 eV are observed on $Mo-V/SiO_2$ (stage 4, 8800 h) (Table 3). They are attributed to Cl^- ions coordinated to molybdenum ions. Their binding energies correspond to those obtained in the literature for molybdenum chlorides.[48] They cannot be attributed to chlorine ions bonded to silica, since, as already mentioned above, HCl chlorinates SiO_2 only above 300 °C.[36] These chlorine ions probably contribute to the change in the speciation of V and the formation of the mixed amorphous phase, which would therefore contain V^{IV}, Mo^{VI}, O^{2-}, and Cl^- ions. This phase will be labeled $V^{IV}-O-Mo^{VI}-Cl$ in the following.

The reduction of V^V to V^{IV} ions is confirmed by EPR spectroscopy. The broadening of the V^{IV} signal, ΔH_{pp}, from ∼100 G before reaction (**VS1**) (Figure 4a) to 800 G after 8800 h of reaction (**VS4″**) (Figure 4i) indicates an increase in the dipolar interaction between the V^{IV} ions. The low percentage of V^{IV} ions detected by EPR (Figure 3) (∼0.2% of the overall V ions) may also indicate that a large number of V^{IV} ions forms $V^{IV}-O-V^{IV}$ pairs, which are not visible by EPR because of line broadening.

TABLE 6: Intervalence Charge-Transfer Transitions in One-Electron- and Two-Electron-Reduced Compounds Containing V^{IV} and/or Mo^V Ions[a]

compound	band positions (nm)	IVCT assignment	ref
polyvanadic acid gel	1410, 1515	$V^{IV}-V^V$	51
α-$[SiMoV_2W_9O_{40}]^{7-}$	1090	$V^{IV}-V^V$	52
α-$[PMoV_2W_9O_{40}]^{6-}$	1110	$V^{IV}-V^V$	52
$[Mo_6O_{19}]^{3-}$	1110 sh	Mo^V-Mo^{VI}	53
α-$[PMo_{12}O_{40}]^{4-}$	1160 sh, 1560 sh	Mo^V-Mo^{VI}	53
α-$[SiMo_{12}O_{40}]^{5-}$	1430 sh	Mo^V-Mo^{VI}	53
α-$[PVMo_{11}O_{40}]^{5-}$	660	$V^{IV}-Mo^{VI}$	1
α-$[SiVMo_{11}O_{40}]^{6-}$	640	$V^{IV}-Mo^{VI}$	1
α-$[SiMoV_2W_9O_{40}]^{8-}$	460 sh	$V^{IV}-W^{VI}$	52
	530	$V^{IV}-Mo^{VI}$	
α-$[PMo_2VW_9O_{40}]^{5-}$	480	$V^{IV}-W^{VI}$	52
	625	$V^{IV}-Mo^{VI}$	

[a] sh = shoulder.

No d−d transition band of V^{IV} ions expected in the range ∼600−850 nm[47,49,50] is clearly observed (Figure 6d). Only a very weak band at 900 nm is visible when the spectrum is enlarged (see the inset in Figure 6d). The only difference with the initial spectrum (Figure 6a) is the presence of an additional shoulder at ∼550 nm, which may attest the presence of a $V^{IV} \rightarrow Mo^{VI}$ intervalence charge-transfer (IVCT) transition (Table 6). This result seems to indicate that Mo has diffused into the bulk of the V_2O_5 crystallites.

The coverage of silica by vanadium increases during the reaction. Indeed, the V/Si atomic ratio increases from 0.19 for V/SiO_2 to 0.42 for $Mo-V/SiO_2$ (8800 h) (Table 3), suggesting that the mixed $V^{IV}-O-Mo^{VI}-Cl$ phase spreads over the silica surface during the reaction. This is consistent with the amorphization of the supported phase deduced from the Raman spectra and the STEM micrographs. The spreading of the mixed $V^{IV}-O-Mo^{VI}-Cl$ phase is also attested by the decrease in the intensity of the SiO−H vibration bands at 1350 and 2200 nm (Figure 6). It is noted that Reddy et al.,[54] who prepared Mo-promoted VO_x/SiO_2 by impregnation of VO_x/SiO_2 with molybdenum heptamolybdate followed by calcination at 500 °C, reported that "under the influence of MoO_3 the vanadia phase spreads more and covers more support surface". However, the authors did not characterize the supported phase.

After the $Mo-V/SiO_2$ sample (8800 h) is washed with water, the V and Mo loadings decrease in the same proportion, since the V/Mo atomic ratio remains equal to ∼4. This indicates that (i) the supported $V^{IV}-O-Mo^{VI}-Cl$ phase is soluble in water, (ii) Mo and V are intimately associated and homogeneously distributed in the supported phase of the $Mo-V/SiO_2$ sample, and (iii) the nature of the supported phase does not seem to change upon washing.

c. Evolution of V/SiO₂ during the Former Stages of Reaction with MoCl₅. Now, we will attempt to ascribe stage by stage the changes observed in the EPR and UV−vis−near-IR spectra of the V/SiO_2 sample during the reaction with $MoCl_5$ at 30 °C, to understand how V_2O_5 transforms into the mixed $V^{IV}-O-Mo^{VI}-Cl$ amorphous phase.

Stage 1:

After calcination, V^{IV} ions in dipolar interaction are present on the surface of V_2O_5 in the V/SiO_2 sample, as indicated by the broad **VS1** signal (Figure 4a, Table 2). Within the first 20 h of reaction (stage 1), the absence of a change in the shape and in the intensity of the EPR signal (Figures 3 and 4a) suggests that $MoCl_5$ does not react with V/SiO_2. However, since the Mo^V concentration after 20 h of reaction with bare silica (1×10^{17} spins·g^{-1}, Figure 2) is lower than the initial V^{IV} concentration

in V/SiO_2 (1×10^{18} spins·g^{-1}, Figure 3), a possible reaction of $MoCl_5$ with silica uncovered by V_2O_5 cannot be discarded.

Stage 2:

During stage 2, the sample turns green upon reduction of V^V to V^{IV}, as indicated by the increase in the V^{IV} spin concentration (Figure 3) and the appearance of a broad d−d band of V^{IV} ions[47,49,50] at ∼800−900 nm (Figure 6b). The coexistence of this d−d band and of the $O^{2-} \rightarrow V^{5+}$ charge-transfer bands is responsible for the green color. The V^{IV} EPR spectrum shape is different from that of stage 1. Signal **VS2** of V^{IV} in axial symmetry with a hyperfine structure is superimposed on the former broad line **VS1** (Figure 4b and Table 2). This rather well-resolved signal associated with an increase in the V^{IV} spin concentration indicates the reduction of V^V to V^{IV} ions without spin−spin interaction. The EPR parameters of signal **VS2** are close to those of amorphous V_2O_5 ($g_\perp = 1.980$, $g_\parallel = 1.913$, $a_\perp = 66$ G, $a_\parallel = 176$ G)[55] or of crystallized V_2O_5 ($g_\perp = 1.986$, $g_\parallel = 1.923$, $a_\perp = 62$ G, $a_\parallel = 168$ G).[56] This suggests that the crystal field around V^{IV} is a square pyramidal VO_5 with a short V−O bond along the *z* axis. In addition, it was observed that the hyperfine structure of signal **VS2** broadens, decreases in intensity, and disappears after O_2 adsorption (∼5 Torr) at room temperature. This indicates that the corresponding V^{IV} ions are located on the V_2O_5 surface. According to Busca et al.,[57] V_2O_5 contains surface hydroxyl groups; the free OH groups disappear after evacuation at 110 °C, whereas the H-bonded OH groups resist evacuation at 300 °C, and correspond to Bronsted sites evidenced by adsorption of pyridine[57] and ammonia.[58] Hence, it is proposed that the reduction of surface V^V to V^{IV} ions arises from an electron transfer from Mo^V to V^V ions, as already proposed for stage 4 (reaction VI), and results from a reaction between $MoCl_5$ and surface OH groups of V_2O_5:

$$V^V{-}OH + Mo^VCl_5 \rightarrow V^{IV}{-}O{-}Mo^{VI}Cl_4 + HCl \quad \text{(VII)}$$

It is noted that no Mo^V EPR signal is observed on Mo−V/SiO_2 (86 h) (Figure 4b). However, it is possible that it is hidden by the V^{IV} signal. In this case, it should be very weak since the Mo^V EPR signal visible in Mo/SiO_2 (88 h) (Figure 1b) is 50 times smaller (Figure 2) than that of V^{IV} ions on Mo−V/SiO_2 (Figure 3). The UV−vis spectrum (Figure 6b) does not help either in the evidence of Mo^V ions since its d−d transition[47,49,59] is in the same range as that of the V^{IV} ions (∼800−900 nm).[47,49,50]

It is also proposed that V^V ions are reduced to V^{IV} ions by the HCl formed during reaction VII, according to the following reaction:

$$V^V{=}O + 2HCl \rightarrow V^{IV}{-}Cl + {}^1/_2Cl_2 + H_2O \quad \text{(VIII)}$$

The same type of reaction has already been proposed by Abdo et al.[60] to explain the reduction of $Mo^{VI}{=}O$ to $Mo^V{-}Cl$ species in MoO_3 supported on γ-alumina in the presence of HCl. We checked that HCl adsorption at 30 °C on V/SiO_2 induces an increase in the V^{IV} EPR signal (from 0.2% to 0.5% of the V ions) and the appearance of a hyperfine structure superimposed on the initial **VS1** broad line.

The small decrease in the V^{IV} EPR signal between 300 and 500 h of reaction (Figure 3), accompanied by the disappearance of signal **VS2**, could be due to the increasing interaction between surface V^{IV} ions (Figure 4c). This would mean that more V^V ions are reduced to V^{IV}, and that the concentration of V^{IV} measured by EPR is smaller than the real one because of the signal broadening.

TABLE 7: EPR Parameters of V^{IV} Compounds

compound	$g_\perp$	$g_\parallel$	$a_\perp$ (G)	$a_\parallel$ (G)	ref
$V_2O_5{-}MoO_3$ solid solution	1.99	1.90	49	144	4
one-electron-reduced					
Keggin heteropolyanions					
α-$[PVMo_{11}O_{40}]^{5-}$	1.974	1.939	53	151	1
α-$[SiVMo_{11}O_{40}]^{6-}$	1.975	1.936	54	149	
V^{IV} in tetrahedral coordination					
$Ga_2NaMg_2V_3O_{12}$	1.980	1.855	32	175	61
tetrakis-*tert*-butoxy ($V(OR)_4$)	1.984	1.94	39	138	62
vanadium tetramethoxide	1.985	1.955	30	137	63
V^{IV} in $ThGeO_4$	1.980	1.831	34	194	64
one-electron reduced					
Dawson heteropolyanion					
$[HP_2V_3W_{15}O_{62}]^{9-}$	1.957	1.942	45	134	65

Stage 3:

During stage 3 (500−2500 h), the sample turns black, and the intensity of the V^{IV} EPR signal drastically increases (Figure 3), to correspond to the reduction of up to 20% of the overall V ions. This may indicate that the reduction takes place in the bulk of V_2O_5 by electron transfer from Mo^V ions.

Meanwhile, the UV−vis−near-IR spectrum shows a broadening of the CT band toward the higher wavelength (Figure 6c) attributed to the presence of a $V^{IV}{-}Mo^{VI}$ IVCT transition (Table 6), as also observed during stage 4 (Figure 6d). It also exhibits a broad absorption at ∼1175 nm, which could be attributed to a $V^{IV}{-}V^V$ or a $Mo^V{-}Mo^{VI}$ IVCT transition (Table 6). However, the absence or the very weak intensity of the Mo^V signal in the EPR spectrum leads to the conclusion that the band at 1175 nm rather arises from a $V^{IV}{-}V^V$ IVCT transition. The higher intensity of the V^{IV} d−d transition band at ∼840 nm (Figure 6c) than in stage 2 (Figure 6b) is probably due to the underlying broad intervalence transition. Hence, the black color of the sample is due to the strong absorption in the whole visible range.

Between ∼500 and 1000 h of reaction, a new V^{IV} signal, **VS3**, appears with a hyperfine structure (Figure 4d). It disappears after 1000−2500 h of reaction (Figure 4e,f). A broad signal, **VS4** ($\Delta H_{pp} = 500$ G), remains visible, indicating that the V^{IV} ions interact with each other, and the V^{IV} signal intensity continues to increase (Figure 3). We could not find any V^{IV}-containing compounds in the literature with EPR parameters close to those of **VS3** ($g_\perp = 1.941$, $g_\parallel = 1.936$, $a_\perp = 13$ G, $a_\parallel = 147$ G, Table 2). The **VS3** parameters are different from those of the V^{IV} ions in $V_2O_5{-}MoO_3$ solid solution and in one-electron-reduced heteropolyanions of Keggin structure, and from those of V^{IV} in tetrahedral coordination (Table 7). The closest parameters are those of $[HP_2V_3W_{15}O_{62}]^{9-}$ of Dawson structure (Table 7), but the $a_\perp$ values are different.

The reaction of one $MoCl_5$ molecule with one oxygen atom of the equatorial plane of vanadium ions would lead to an orthorhombic V^{IV} signal, except if four $MoCl_5$ molecules could react with the four oxygen atoms of the equatorial plane, which is unlikely. It is tentatively proposed that the axial **VS3** signal arises from the reaction of $MoCl_5$ with the oxygen of the vanadyl bond:

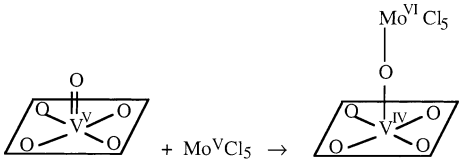

V^{IV}-O-Mo^{VI}-Cl_5 species (IX)

This implies the migration of $MoCl_5$ inside the V_2O_5 crystallites, which is consistent with the fact that an amorphous mixed phase forms during the next stage.

Stage 4:

From the characterization of $Mo-V/SiO_2$ during stages 1−3, new information can be drawn from the EPR spectra obtained during stage 4 (Figure 4g−i). The drastic decrease in the EPR spectrum intensity during this stage (Figure 3) is associated, first, with the reappearance of the **VS3** signal superimposed on a broad signal, **VS4″**, between about 2500 and 3000 h of reaction (Figure 4g) and, second, with its disappearance and the broadening of the remaining EPR signal of V^{IV} ions (ΔH_{pp} = 800 G, Figure 4i). This is due to the fact a larger number of V^{IV} ions interact with each other since all the V^V ions are reduced to V^{IV} ions, as attested by the XPS results and the disappearance of the $V^{IV}-V^V$ intervalence band at 1175 nm (Figure 6d), which also induces a change in the sample color to red.

The low percentage of V^{IV} ions detected by EPR (~0.2% of the overall V ions) (Figure 3) confirms that the mixed $V^{IV}-O-Mo^{VI}-Cl$ phase is amorphous. Indeed, V^{IV} ions in poorly organized phases are known to be EPR inactive because of local disorders which induce changes in the $V^{IV}-V^{IV}$ distances, weaken exchange interactions, and thus prevent EPR detection.[19]

Beyond 3000 h of reaction, a weak EPR signal of Mo^V ions (g_{iso} = 1.947, ΔH_{pp} = 50 G) is also observed (Figure 4h,i). It is attributed to Mo^V ions located on the silica surface. Indeed, the hyperfine structure of the signal (Figure 4i) is similar to that observed on silica after the reaction with $MoCl_5$ (Figure 1c). However, the main line at g_{iso} = 1.947 is broader: ΔH_{pp} = 50 G on $Mo-V/SiO_2$ (Figure 4i) instead of ΔH_{pp} = 37 G on Mo/SiO_2 (Figure 1). This broadening is tentatively explained by the interaction between the Mo^V ions on silica and neighboring V^{IV} ions. It is proposed that the Mo^V signal increases (Figure 3) and becomes predominant (Figure 4h,i) when the mixed $V^{IV}-O-Mo^{VI}-Cl$ phase is "saturated" in Mo (atomic ratio V/Mo = 4).

Initially, the coverage of silica by vanadium in V/SiO_2 is low since the V/Si atomic ratio is equal to 0.19. If $MoCl_5$ had randomly reacted with silica or V_2O_5, it would have given rise to the EPR signals of both V^{IV} and Mo^V ions. This is not observed, which indicates that $MoCl_5$ preferentially reacts with V_2O_5 rather than with silica.

It is noted that at least one point remains unclear: how to explain that 100% of the V^V is reduced to V^{IV} since the atomic ratio V/Mo = 4. This means that there is another source of electrons to reduce V^V other than Mo^V. If HCl also induces the reduction of V^V to V^{IV}, one can suggest that several HCl molecules form during reaction VII.

3. Redox Potentials. Our results show that V^V of monomeric grafted vanadyl species does not react with $MoCl_5$ in contrast with V^V of V_2O_5 microcrystallites, which is reduced to V^{IV} by electron transfer from Mo^V at the gas−solid interface in agreement with the values of the redox potentials of the VO_2^+/VO^{2+} (1 V/NHE) and MoO_2^{2+}/MoO^{3+} (0.48 V/NHE) couples in solution.[2,3] One may wonder why an electron transfer occurs in the case of V^V of V_2O_5, and not of monomeric vanadyl species grafted onto silica.

The literature data show that the redox potentials are in fact very sensitive to several factors.

(1) Symmetry of the complex. In an electrochemical study in solution of the one-electron reduction of heteropolymolybdovanadate complexes ($[H_{n-1}V(V_nMo_{12-n})O_{40}]^{4-}$ with $1 \le n \le 3$) containing both octahedral and tetrahedral V^V, Himeno et al.[66] showed that the octahedral V^V could be reduced whereas the tetrahedral V^V sites were not electrochemically active. On the other hand, Nanda et al.[67] observed for a series of Cu^{II} complexes with the same type of ligands, a $Cu^{II/I}$ redox potential for the complex in tetrahedral symmetry more positive (shift of 250 mV) than for the complex in square planar symmetry.

(2) Nature of the ligands. The ligands can also drastically modify the values of the redox potentials. This is observed for many complexes in solution. In the case of $Ni(CO)_3L$ complexes (L = phosphine) with the same symmetry,[68] the variation of the redox potential may reach 500 mV depending on the nature of the phosphine ligand. It was also shown for $Cu^{II/I}$ complexes[69] that the redox potential varies within a range of 1.5 V depending on the type of ligand, and linearly with the logarithm of the $Cu^{II}L$ stability constant.

(3) Particle size. Due to the confinement of electrons and holes within a very small volume, the particle size (in the 10−100 Å range) also greatly affects the redox potential.[70−72] Thus, in the case of zinc oxide particles, a negative shift of the redox potential larger than 300 mV was observed when the size of the particles decreased from 55 to 30 Å.[70] Such a quantum size effect on the redox potential was first predicted by Brus[71] for small semiconductor crystallites with a simple model called "particle in a box", and then confirmed with experiments on CdS nanoparticles.[72] A similar conclusion was reported by Mostafavi et al.[73,74] for silver aggregates. The electrochemical potential of the couple Ag_n^+/Ag_n (n = aggregate nuclearity) increases by more than 2 V for n increasing from 1 to 10.

As a consequence, the values of the redox potentials of a given ion of an oxide particle or of a monomeric species are not easily predictable from the usual solution values of the literature and may be very different from one to the other (>500 mV). In addition, the redox potential may depend on the species state (liquid, solid, or gas) and on the nature of the interface (liquid−solid, gas−solid, ...).

As already mentioned, two types of V^V species are present on the silica surface. One of them in V_2O_5 crystallites is octahedral and polymeric with V ions in the second coordination sphere, i.e., with VO^- ligands; the other one is tetrahedral and monomeric and is grafted onto silica (vanadyl species $(\equiv SiO)_3V{=}O$) with SiO^- ligands. It is noted that SiO^- is a supermolecular, chelating, and weak crystal field ligand.[75] In this respect, it belongs to the class of σ donor−π donor ligands[75] such as Cl^- and H_2O, and could be introduced into the spectrochemical series, leading to the following sequence for increasing values of the crystal field parameter:[76]

$$Cl^- < SiO^- < H_2O < NH_3 < NH_2CH_2CH_2NH_2$$

Thus, these two types of V^V species have different ligands, different symmetries, and different nuclearities. Each of these factors induces a shift of the V^V/V^{IV} redox potential, which may be positive or negative relative to the reference solution value. It may be noted, for example, that the V^V/V^{IV} redox potential of V_2O_5 in solution is equal to 0.7 V/NHE,[2] which is a value significantly higher than the 1 V/NHE value of the VO_2^+/VO^{2+} couple in solution.[2,3]

From the present results, i.e., the fact that $MoCl_5$ reacts with the V_2O_5 crystallites but not with the monomeric vanadyl species, the following order of the redox potentials may be proposed:

$$E(V^V/V^{IV})_{V_2O_5\ cryst} > E(Mo^{VI}/Mo^V)_{MoCl_5} > E(V^V/V^{IV})_{(\equiv SiO)_3V=O}$$

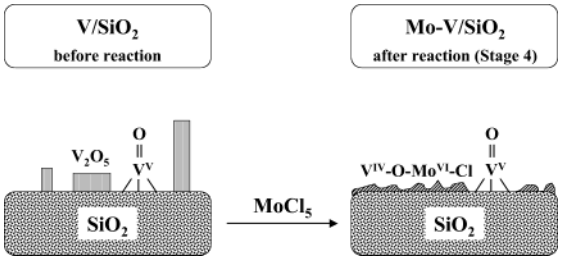

Figure 8. Model for the transformation of the supported vanadium oxide phase into the amorphous mixed $V^{IV}-O-Mo^{VI}-Cl$ phase upon reaction with gas-phase $MoCl_5$ at 30 °C.

Conclusions

An electron transfer at the gas−solid interface is studied by means of the reaction at 30 °C of gas-phase $MoCl_5$ with silica-supported vanadium oxide prepared by impregnation and calcination. An electron transfer accompanied by complex chemical changes of the supported phase is followed over a long period of time (up to 9000 h). The samples are characterized in situ (i.e., in air-free conditions) by various spectroscopies (EPR, diffuse reflectance UV−vis−near-IR, Raman, XPS), chemical analysis, and electron microscopy. The changes in color of the sample define four various stages of reaction: orange before reaction and during stage 1 (0−20 h), green during stage 2 (20−500 h), black during stage 3 (500−2500 h), and finally red during stage 4 (2500−9000 h). They are accompanied by drastic variations in the speciation of vanadium and in the chemical state of the supported phase. Before reaction and during stage 1, the V/SiO_2 sample contains V_2O_5 crystallites and monomeric tetrahedral vanadyl species grafted onto silica ($(\equiv SiO)_3V{=}O$). At the end of stage 1, 0.2% of the vanadium is in the IV oxidation state. During stage 2, 0.3% of the V^V ions are reduced to V^{IV} ions because of the reaction of $MoCl_5$ with V^V ions at the surface of the V_2O_5 crystallites, and an electron transfer from Mo^V to V^V is observed. During stage 3, $MoCl_5$ reacts with the bulk of the V_2O_5 crystallites: 20% of the V^V ions are reduced to V^{IV} ions, and a mixed $V^{IV}-O-Mo^{VI}-Cl_5$ species is formed. During stage 4, the remaining V^V ions are reduced to V^{IV}, and $MoCl_5$ deeply alters the V_2O_5 structure, which is transformed into an amorphous mixed $V^{IV}-O-Mo^{VI}-Cl$ phase (atomic ratio $V/Mo = 4$) spread over the silica surface (Figure 8). The electron transfer from gas-phase $MoCl_5$ to solid V_2O_5 is consistent with the prediction given by the redox potentials of VO_2^+/VO^{2+} and MoO_2^{2+}/MoO^{3+} couples in solution, i.e., $E°(V^V/V^{IV})$ (1 V) > $E°(Mo^{VI}/Mo^V)$ (0.48 V). In contrast, $MoCl_5$ does not significantly react with monomeric tetrahedral vanadyl species grafted onto silica. This leads us to propose the following sequence of redox potentials at the gas−solid interface: $E(V^V/V^{IV})_{V_2O_5\ cryst} > E(Mo^{VI}/Mo^V)_{MoCl_5} > E(V^V/V^{IV})_{(\equiv SiO)_3V=O}$. Such a difference in the behavior of the vanadium species toward electron transfer with $MoCl_5$ can be explained in terms of the dependence of the nature of the ligands, the symmetry, and the nuclearity of the vanadium species on the redox potentials.

Acknowledgment. We warmly thank Prof. G. Hervé (Université de Versailles-Saint Quentin) for helpful discussions on the electron transfer and redox potentials of heteropolyanions.

References and Notes

(1) Altenau, J. J.; Pope, M. T.; Prados, R. A.; So, H. *Inorg. Chem.* **1975**, *14*, 417.
(2) Pourbaix M. *Atlas d'Equilibres Electrochimiques à 25 °C*; Gauthier-Villars: Paris, 1963; p 236.
(3) Bernard, M.; Busnot, F. *Usuel de Chimie Générale et Minérale*; Dunod: Paris, 1996; p 184.
(4) Dyrek, K.; Labanowska, M. *J. Catal.* **1983**, *81*, 46.
(5) Kazanskii, V. B.; Ezhkova, Z. I.; Lyubarskii, A. G.; Voevodskii, V. V.; Ioffe, I. I. *Kinet. Catal.* **1961**, *2*, 783.
(6) Busca, G.; Marchetti, L. *J. Chem. Res., Synop.* **1986**, 174.
(7) Che, M.; Louis, C.; Tatibouët J. M. *Polyhedron* **1986**, *5*, 123.
(8) Louis, C.; Che, M. *J. Catal.* **1992**, *135*, 156.
(9) Louis, C.; Che, M.; Anpo, M. *J. Catal.* **1993**, *141*, 453.
(10) Louis, C.; Che, M. In *Handbook on Heterogeneous Catalysis*; Ertl, G., Knözinger, H., Weitkamp, J., Eds.; VCH: Weinheim, Germany, 1997; Vol. 1, p 207.
(11) Cordischi, D.; Indovina, V.; Occhiuzi, M. *Appl. Surf. Sci.* **1992**, *55*, 233.
(12) Emsley, J. *The elements*; Clarendon Press: Oxford, 1989.
(13) Saeki, Y.; Matsukazi R. *Denki Kagaku* **1965**, *33*, 151.
(14) Dyrek, K.; Madej, A.; Mazur, E.; Rokoz, A. *Colloids Surf.* **1990**, *45*, 135.
(15) Madej, A.; Dyrek, K.; Mattusch, J. *Fresenius' J. Anal. Chem.* **1991**, *341*, 707.
(16) Dyrek, K. Personal communication.
(17) Lozos, G. P.; Hoffman; B. M.; Franz, C. G. QCPE No. 265.
(18) Scofield, J. H. *J. Electron Spectrosc.* **1976**, *8*, 129.
(19) Poole, C. P. *Electron Spin Resonance, A Comprehensive Treatise on Experimental Techniques*, 2nd ed.; Wiley-Interscience: New York, 1983; p 547.
(20) Anderson, J. H.; Wickersheim, K. A. *Surf. Sci.* **1964**, *2*, 252.
(21) Cimino, A.; De Angelis, B. A. *J. Catal.* **1975**, *36*, 11.
(22) Masson, J.; Nechtschein, J. *Bull. Soc. Chim. Fr.* **1968**, 3933.
(23) Wagner, C. D.; Riggs, W. M.; Davis, L. E.; Moulder, J. F.; Muilenberg, G. E. *Handbook of X-ray Photelectron Spectroscopy*, 1st ed.; Physical Electronics Division, Perkin-Elmer Corp.: Eden Prairie, MN, 1979.
(24) Nogier, J. P. *Catal. Today* **1994**, *20*, 109.
(25) Le Coustumer, L. R.; Taouk, B.; Le Meur, M.; Payen, E.; Guelton, M.; Grimblot, J. *J. Phys. Chem.* **1988**, *92*, 1230.
(26) Oyama, S. T.; Went, G. T.; Lewis, K. B.; Bell, A. T.; Somorjai, G. A. *J. Phys. Chem.* **1989**, *93*, 6786.
(27) Deo, G.; Wachs, I. E. *J. Phys. Chem.* **1991**, *95*, 5889.
(28) Galeener, F. L.; Lucovsky, G. *Phys. Rev. Lett.* **1976**, *37*, 1474.
(29) Galeener, F. L.; Sen, P. N. *Phys. Rev.* **1978**, *B17*, 1928.
(30) Galeener, F. L. *Phys. Rev.* **1979**, *B19*, 4292.
(31) Galeener, F. L.; Mikkelsen, J. C., Jr. *Phys. Rev.* **1981**, *B23*, 5527.
(32) Shibata, N.; Horigudhi, M.; Edahira, T. *J. Non-Cryst. Solids* **1981**, *45*, 115.
(33) Bertoluzza, A.; Fagnano, C.; Gottardi, V.; Guglielmi, M. *J. Non-Cryst. Solids* **1982**, *48*, 117.
(34) Hirata, T.; Zhu, H. Y. *J. Phys.: Condens. Matter* **1992**, *4*, 7377.
(35) Che, M.; Fournier, M.; Launay, J. P. *J. Chem. Phys.* **1979**, *71*, 1954.
(36) Haukka, S.; Lakomaa, E. L.; Root, A. *J. Phys. Chem.* **1993**, *97*, 5085.
(37) Brisdon, B. J.; Graham, J. T.; Hope, E. G.; Jenkins, D. M.; Levason, W.; Ogden, J. S. *J. Chem. Soc., Dalton Trans.* **1990**, 1529.
(38) Levason, W.; Narayanaswamy, R.; Ogdsen, J. S.; Rest, A. J.; Turff, J. W. *J. Chem. Soc., Dalton Trans.* **1981**, 2501.
(39) Garner, C. D.; Hill, L. H.; Mabbs, F. E.; McFadden, D. L.; McFail, A. T. *J. Chem. Soc., Dalton Trans.* **1977**, 853.
(40) Manoharan, P. T.; Rogers, M. T. *J. Chem. Phys.* **1968**, *49*, 5510.
(41) Freund, F. *J. Am. Ceram. Soc.* **1967**, *50*, 493.
(42) Louis, C.; Che, M. *J. Phys. Chem.* **1987**, *91*, 2875.
(43) Mériaudeau, P.; Clerjaud, B.; Che, M. *J. Phys. Chem.* **1983**, *87*, 3872.
(44) Abdo, S.; Clarkson, R. B.; Hall, W. K. *J. Phys. Chem.* **1976**, *80*, 2431.
(45) Lunsford, J. H. *Adv. Catal.* **1972**, *22*, 5201.
(46) Hanuza, J.; Oganowski, W.; Jezowska-Trzebiatowska B. *J. Mol. Catal.* **1985**, *29*, 109.
(47) Praliaud, H.; Mathieu, M. V. *J. Chim. Phys.* **1976**, *54*, 689.
(48) Walton, R. A. *J. Less-Common Met.* **1977**, *73*, 71.
(49) Jørgensen, C. K. *Acta Chem. Scand.* **1957**, *11*, 73.
(50) Ballhausen, C. J.; Gray, H. B. *Inorg. Chem.* **1962**, *1*, 111.
(51) Gharbi, N.; Sanchez, C.; Livage, J.; Lemerle, J.; Nejem, L.; Lefebvre J. *Inorg. Chem.* **1982**, *21*, 2758.
(52) Cadot, E.; Fournier, M.; Tézé, A.; Hervé G. *Inorg. Chem.* **1996**, *35*, 282.
(53) Sanchez, C.; Livage, J.; Launay, J. P.; Fournier, M.; Jeannin, Y. *J. Am. Chem. Soc.* **1982**, *104*, 3194.
(54) Reddy, B. M.; Narsimha, K.; Rao, P. K.; Mastikhin, V. M. *J. Catal.* **1989**, *118*, 22.
(55) Nabavi, M.; Sanchez, C.; Livage, J. *Philos. Mag. B* **1991**, *63*, 941.
(56) Kahn, A.; Livage, J.; Collongues, R. *Phys. Status Solidi* **1974**, *1*, 175.
(57) Busca, G.; Ramis, G.; Lorenzelli, V. *J. Mol. Catal.* **1989**, *50*, 231.
(58) Topsoe, N. Y. *J. Catal.* **1991**, *128*, 499.

(59) Horner, S. M.; Tyree, S. Y., Jr. *Inorg. Chem.* **1963**, *2*, 568.
(60) Abdo, S.; Kazusaka, A.; Howe, R. F. *J. Phys. Chem.* **1981**, *85*, 1380.
(61) Oversluizen, G.; Metselaar, R. *J. Phys. C: Solid State Phys.* **1982**, *15*, 4869.
(62) Kokoschka, G. F.; Allen, H. C., Jr.; Gordon, G. *Inorg. Chem.* **1966**, *5*, 91.
(63) Bradley, D. C.; Moss, R. H.; Sales, K. D. *Chem. Commun.* **1969**, 1255.
(64) Di Gregorio, S.; Greenblatt, M.; Pifer, J. H.; Sturge, M. D. *J. Phys. Chem.* **1982**, *76*, 2931.
(65) So, H.; Pope, M. T. *Stud. Phys. Theor. Chem.* **1992**, *78*, 71.
(66) Himeno, S.; Osakai, T.; Saito, A. *Bull. Chem. Soc. Jpn.* **1991**, *64*, 21.
(67) Nanda, K. K.; Addison, A. W.; Butcher, R. J.; McDevitt, M. R.; Rao, T. N.; Sinn, E. *Inorg. Chem.* **1997**, *36*, 134.
(68) Suresh, C. H.; Koga, N. *Inorg. Chem.* **2002**, *41*, 1573.
(69) Ambundo, E. A.; Deydier, M. V.; Grall, A. J.; Aguera-Vega, N.; Dressel, L. T.; Cooper, T. H.; Heeg, M. J.; Ochrymowycz, L. A.; Rorabacher, D. B. *Inorg. Chem.* **1999**, *38*, 4233.
(70) Hoyer, P.; Weller, H. *Chem. Phys. Lett.* **1994**, *221*, 379.
(71) Brus, L. E. *J. Chem. Phys.* **1983**, *79*, 5566.
(72) Haram, S. K.; Quinn, B. M.; Bard, A. J. *J. Am. Chem. Soc.* **2001**, *123*, 8860.
(73) Mostafavi, M.; Marignier, J. L.; Amblard, J.; Belloni, J. *Radiat. Phys. Chem.* **1989**, *34*, 605.
(74) Mostafavi, M.; Marignier, J. L.; Amblard, J.; Belloni, J. *Z. Phys. D* **1989**, *12*, 31.
(75) Che, M. *Stud. Surf. Sci. Catal.* **1993**, *75A*, 31.
(76) Lepetit, C.; Che, M. *J. Mol. Catal.* 1**995**, *100*, 147.